Journal of New Materials for Electrochemical Systems 18, 009-016 (2015)

Effect of Structural and Electrochemical Properties of Yttrium-doped $LiNi_{0.90}Co_{0.05}Al_{0.05}O_2$ Electrode by Co-precipitation for Lithium Ion-batteries

Gi-Won Yoo, Tae-Jun Park , Jong-Tae Son*

Department of Nano-Polymer Science & Engineering,
Korea National University of Transportation Chungju, Chungbuk 380-702, Republic of Korea

Received: June 15, 2014, Accepted: November 15, 2014, Available online: February 09, 2015

Abstract: *In this study, the $LiNi_{0.90-x}Co_{0.05}Al_{0.05}Y_xO_2$ (x = 0, 0.025, 0.075) have been synthesized by a co-precipitation and solid-state reaction method. The effect of the Y^{3+}-doping on the structural and electrochemical properties were investigated by X-ray diffraction (XRD), scanning electron microscopy (SEM), and by electrochemical and impedance spectroscopy (EIS). From the results of the XRD pattern changes between before and after the doping, less cation mixing and more ordered hexagonal structure were observed for the $LiNi_{0.875}Co_{0.05}Al_{0.05}Y_{0.025}O_2$ cathode and the cell delivered an initial discharge capacity of 195.8 $mAhg^{-1}$ and was 10.2 $mAhg^{-1}$ higher than the pristine cell by yttrium doping effect. High rate capability studies were also performed and showed the capacity retention of 95, 81.7 and 63.8 % at 0.2, 1.0 and 5.0 C-rate, respectively during the cycling. The impedance spectra showed that the charge transfer resistance for the pristine cathode grew significantly, while that for the Y^{3+}-doped cathode decreased during cycling. It was concluded that the capacity fading for $LiNi_{0.90}Co_{0.05}Al_{0.05}O_2$ mainly due to the cation mixing, partially contributed by the impedance growth and by doping the pristine material with Y^{3+}, cation mixing can be efficiently suppressed, which results in the improved rate capability.*

Keywords: $LiNi_{0.9}Co_{0.05}Al_{0.05}O_2$; Lithium ion battery; Cathode material; Co-precipitation; Yttrium; Electrochemical properties

1. INTRODUCTION

Among the various cathode materials that have been used in lithium batteries, $LiCoO_2$ [1-6] has been mainly used for commercial applications due to its superior electrochemical stability [4]. However, the $LiCoO_2$ cathode has several limitations in terms of its high cost, toxicity, and low capacity. As an alternative, $LiNiO_2$ has been developed for cost reduction and to circumvent the environmental issues by replacing Co with Ni [7], however, this material has low thermal stability, a poor cycle life in the charged state and is difficult to synthesize. It has been known that the cationic substitution in $LiNiO_2$ can be performed to improve electrochemical reactivity [30-33], and these materials, Co and Al co-doped $LiNiO_2$-based materials, $LiNiCoAlO_2$, are attractive because they show relatively better thermal stability and cyclability than $LiNiO_2$ [8]. Thus, the battery performances of lithium-ion cells with a $LiNi_{0.90}Co_{0.05}Al_{0.05}O_2$ cathode are better than cells with $LiNiO_2$. However, it has been reported that $LiNi_{0.90}Co_{0.05}Al_{0.05}O_2$ still shows capacity fading and an increase in resistance after cycling tests [9].

*To whom correspondence should be addressed: Email: jt1234@ut.ac.kr

Ion doping is an effective means of modifying the electronic structure and improved the electrochemical performances. So far, elements such as Fe and Mg [10] have been reported for partial substitution of Ni to reduce the cation mixing and improve the rate capability of the cathode materials [11, 12]. So, substitution of Ni in the Ni-based oxide may be a good method to modify the structural and electrochemical performance of these materials. Therefore, Y^{3+} was chosen as the doping element because it has a larger ionic radius than Ni^{2+},and because Y^{3+} can increase the electronic conductivity and help in the electronic charge transfer during intercalation/deintercalation of Li^+ ion [13,14].

In this paper, we described the investigation of substituting Y^{3+} for Ni^{2+} ion in $LiNi_{0.90}Co_{0.05}Al_{0.05}O_2$ in targeting to improve rate capability and reduced charge transfer resistance of the electrode after cycling.

2. EXPERIMENTAL

$LiNi_{0.90-x}Co_{0.05}Al_{0.05}Y_xO_2$ (x = 0, 0.025, 0.075) materials were prepared by co-precipitation method from stoichiometric amounts of $NiSO_4{\cdot}6H_2O$, and $CoSO_4{\cdot}7H_2O$, were mixed. A spherical $Ni_{0.95}Co_{0.05}(OH)_2$ precursor was prepared through a co-

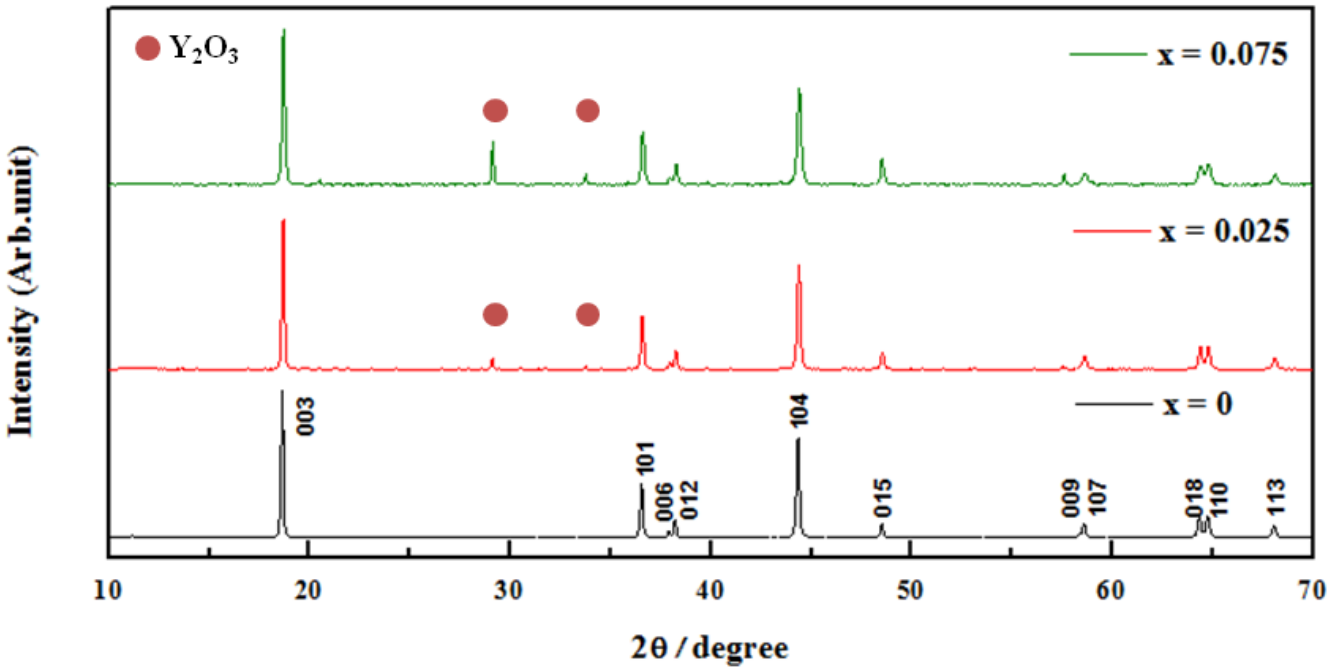

Figure 1. The XRD patterns of the $LiNi_{0.90-x}Co_{0.05}Al_{0.05}Y_xO_2$ (x = 0, 0.025, 0.075) materials.

precipitation process in a continuously stirred tank. At first, stoichiometric amount of metal solution at a concentration of 2 mol L^{-1} was pumped into a continuously stirred tank reactor (CSTR, 4L) under a N_2 atmosphere. At the same time, a NaOH solution (aq) of 2 mol L^{-1} and the desired amount of a NH_4OH solution (aq.) as a chelating agent were also separately pumped into the reactor. The pH of the whole reaction process was kept at 11.0. The obtained $Ni_{0.95}Co_{0.05}(OH)_2$ precursor was thoroughly mixed and ball-milled for at least 24 hrs with an appropriate amount of LiOH, Y_2O_3 nanopowder (<50 nm, Aldrich) (x = 0, 0.025, 0.075 mol *%* ratio in total cation) and $Al(OH)_3.H_2O$ calcined 750 ˚C for 18 hrs in O_2 atmosphere. However, a slightly excess stoichiometry of lithium (1.04) was used to compensate for any loss of the metal that might have occurred during the firing at high temperature.

X-ray diffraction (XRD) patterns were obtained with an X-ray a diffractometer in the 2θ range from 10 to 70° and with monochromatic Cu-Kα radiation (λ = 1.5406 Å). Samples were investigated with scanning electron microscopy (SEM QUANTA 300, JEOL) analysis before and after doping.

CR2016 type coin cells were assembled in a glove box using the above cathode film, lithium, a porous polyethylene film, and a 1M $LiPF_6$ solution in ethylene carbonate (EC) / diethyl carbonate (DEC)(1:1 vol/vol). The lithium metal foil was used as the counter and reference electrode. Assembly was measured in an argon-filled glove box. The charge - discharge curves were measured in the voltage range 3.0 to 4.4 V. Impedance spectroscopy was carried out at room temperature using frequencies ranging from 0.01 Hz to 0.1 MHz and alternating-current amplitude of 10 mV. Nyquist plots (Z' vs –Z") were drawn and analyzed using Zplot and Zview software.

3. RESULTS AND DISCUSSION

3.1. Powder characterization

3.1.1. Analysis of the morphology of Y^{3+}-doped $LiNi_{0.90-x}Co_{0.05}Al_{0.05}Y_xO_2$ by XRD

The XRD patterns of $LiNi_{0.90-x}Co_{0.05}Al_{0.05}Y_xO_2$ (x = 0, 0.025, 0.075) materials are shown in Fig. 1. The lattice parameters shown in Table 1 were calculated using XRD analysis software (TOPAS 4.1). All peaks corresponded to a layered α-$NaFeO_2$ structure of space group R-3m. However, some low intensity bands appeared after doping Y^{3+} ions at a high level, which was attributed to Y_2O_3

Table 1. The lattice parameter, R-factor and peak ratio (003) to (104) in the $LiNi_{0.90-x}Co_{0.05}Al_{0.05}Y_xO_2$ (x = 0, 0.025, 0.075).

Composition	Lattice parameter		Cell volume(Å)	(003)/(104)	R-factor
	a(Å)	c(Å)			
x = 0	2.8726 (±0.0001)	14.1936 (±0.0006)	101.43 (±0.01)	1.1072	0.4326
x = 0.025	2.8743 (±0.0001)	14.1965 (±0.0008)	101.57 (±0.01)	1.1235	0.4306
x = 0.075	2.8744 (±0.0001)	14.1966 (±0.0009)	101.58 (±0.01)	1.1681	0.4586

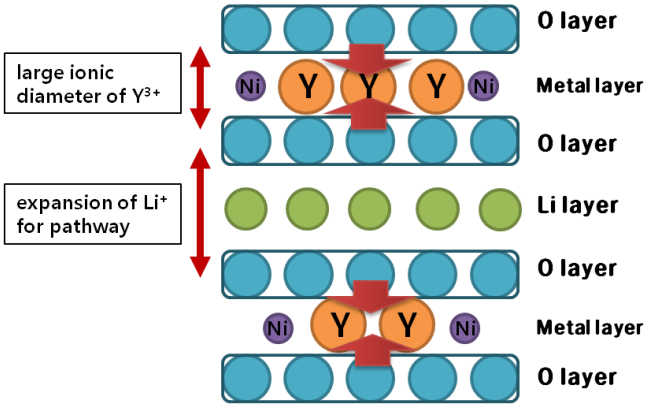

Figure 2. Effect of yttrium on structure

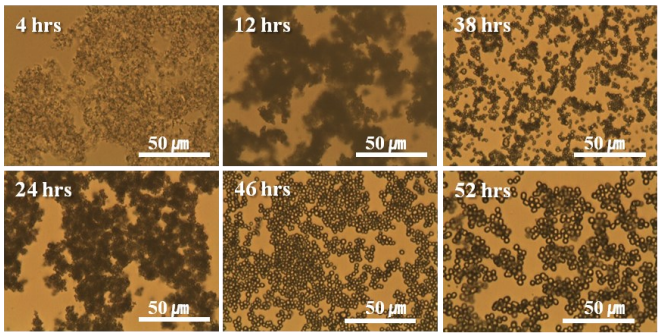

Figure 3. Microscope images of the $Ni_{0.95}Co_{0.10}(OH)_2$ precursor.

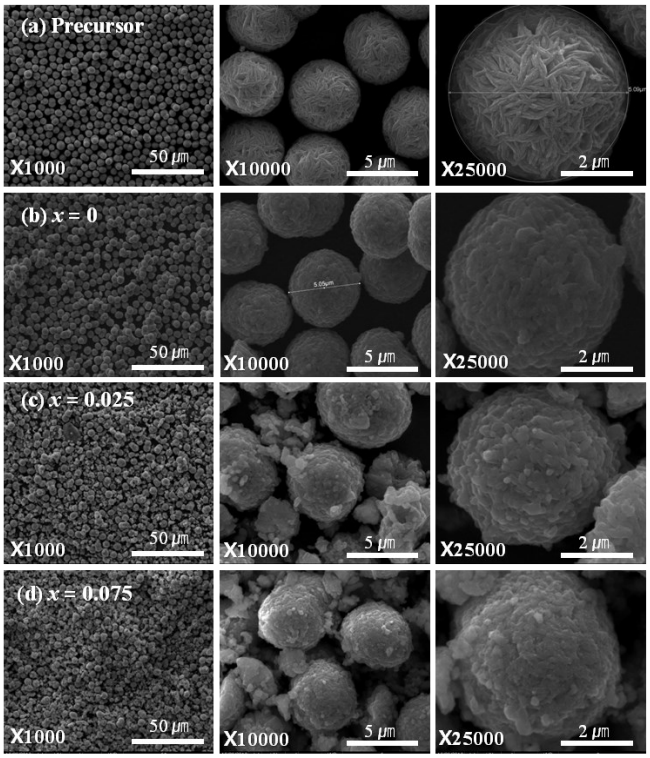

Figure 4. SEM images of the (a) $Ni_{0.95}Co_{0.10}(OH)_2$ precursor and $LiNi_{0.90-x}Co_{0.05}Al_{0.05}Y_xO_2$ powders (x = 0, 0.025, 0.075).

phase formation [15]. Table 1 shows the lattice constants and the intensity ratio of the (003) peak and (104) peak (I(003) / I(104)), which in order to evaluate crystal structure differences after doping. The lattice parameter 'a' represents metal–metal interlayer distance while 'c' indicates the interlayer spacing. The 'a' change in lattice parameters means that the foreign dopant has been incorporated into the crystal structure [16, 17]. In the present study, lattice constants and the I(003)/I(104) ratio changed slightly after doping, indicating that Y^{3+} primarily occupies location of Ni^{2+} crystal lattice sites. Relatively little Y^{3+} was associated with Y_2O_3, phase formation, in Y^{3+}-doped $LiNi_{0.90}Co_{0.05}Al_{0.05}O_2$. The lattice parameters of $LiNi_{0.90-x}Co_{0.05}Al_{0.05}Y_xO_2$ (x = 0.025, 0.075) were larger the compared to that of pristine sample. It indicates that the Y^{3+} ion entered into crystal lattice. The increase in the lattice constant 'a' and 'c' was attributed to the larger ionic diameter of Y^{3+} (radius = 0.90Å versus 0.69Å for Ni^{2+}) [18].

The Y^{3+} doping suggests that the pathway for Li^+ to intercalate/deintercalate had been expanded, which likely occurred because the Y–O bond energy is considerably stronger than the Ni–O bond energy (shown in Fig. 2) [18]. Therefore, the I(003)/I(104) ratio has been used as an indicator of cation mixing [19], that is, values lower than 1.3 indicate a high degree of cation mixing, due to occupancy by other ions in the lithium layer [20]. On the other hand, the higher this ratio is, the lower the degree of ion mixing. In this study, the I(003)/I(104) ratio after Y^{3+} doping was shown to increase, which implies that Ni ions in the lithium layer were depressed by Y-substitution. According to Riemers *et al*. [21], the *R*-factor, which is defined as the ratio of the sum of the intensities of the hexagonal characteristic doublet peaks (0 0 6) and (0 1 2) to that of (1 0 1) peak can be utilized to estimate hexagonal ordering [(I(0 0 6) + I(0 1 2))/I(1 0 1)], and the lower the *R*-factor, the better the hexagonal ordering. In this study, the *R*-factors of $LiNi_{0.90-x}Co_{0.05}Al_{0.05}Y_xO_2$ (x = 0.025) were low than the pristine samples, which means that Y^{3+} doping had a strong structural ordering effect. One of probable reason for this phenomenon was, some low intensity bands appear while the amount of doping Y^{3+} ions increase to a high level, which is attributed to the forming of Y_2O_3 phase (see Fig. 1), while Y-doped sample (x = 0.075) sudden increase in *R*-factor was observed. The reason of this phenomenon is an increase in the amount of the impurities by increasing the amount of yttrium doping, which is believed to hinder the hexagonal ordering.

3.1.2. Microscope of $Ni_{0.95}Co_{0.05}(OH)_2$ precursor

Fig. 3 shows the microscope images of the $Ni_{0.95}Co_{0.05}(OH)_2$ precursor. Co-precipitation of $Ni_{0.95}Co_{0.05}(OH)_2$ was carried out continuously in a CSTR reactor and the change in morphology of the products was monitored regularly by an optical microscope. At the beginning of the reaction, small primary particles were formed and which agglomerate in succession to form irregularly-shaped and micron-sized agglomerates. The particles grew gradually and adopted a uniform spherical morphology without further agglomeration. After 46 hrs of precipitation, a steady state was reached and

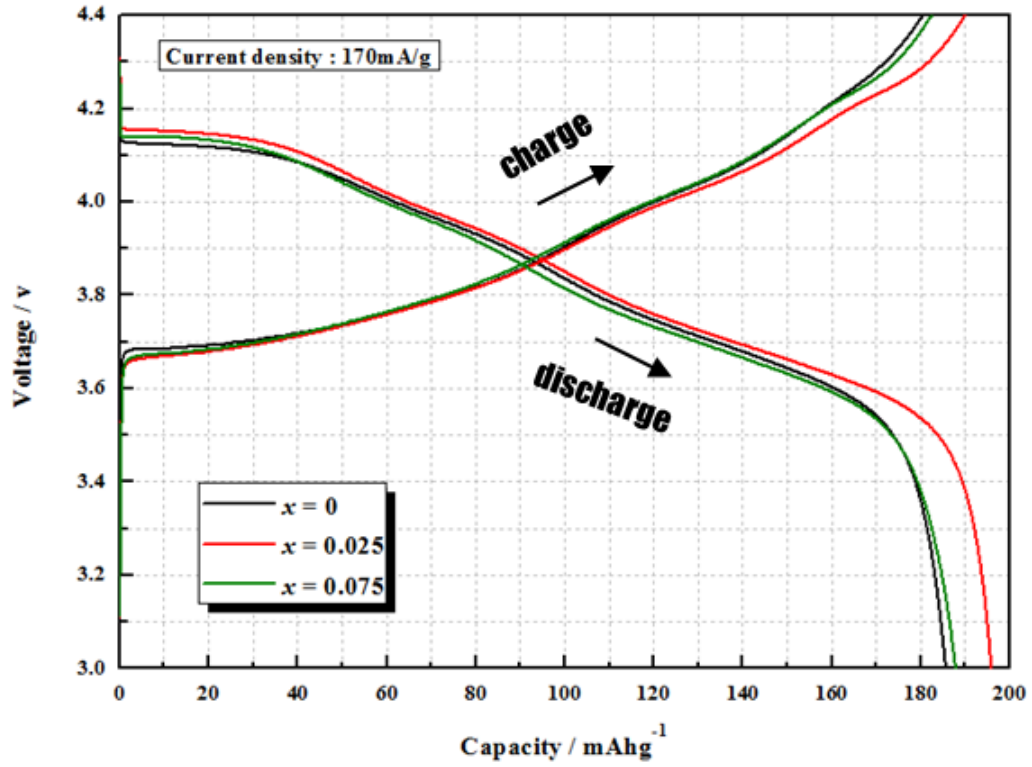

Figure 5. Initial charge-discharge curves of the $LiNi_{0.90-x}Co_{0.05}Al_{0.05}Y_xO_2$ (x = 0, 0.025, 0.075) cathodes in the voltage range of 3.0~4.4 V at 1.0 C (170 mAg).

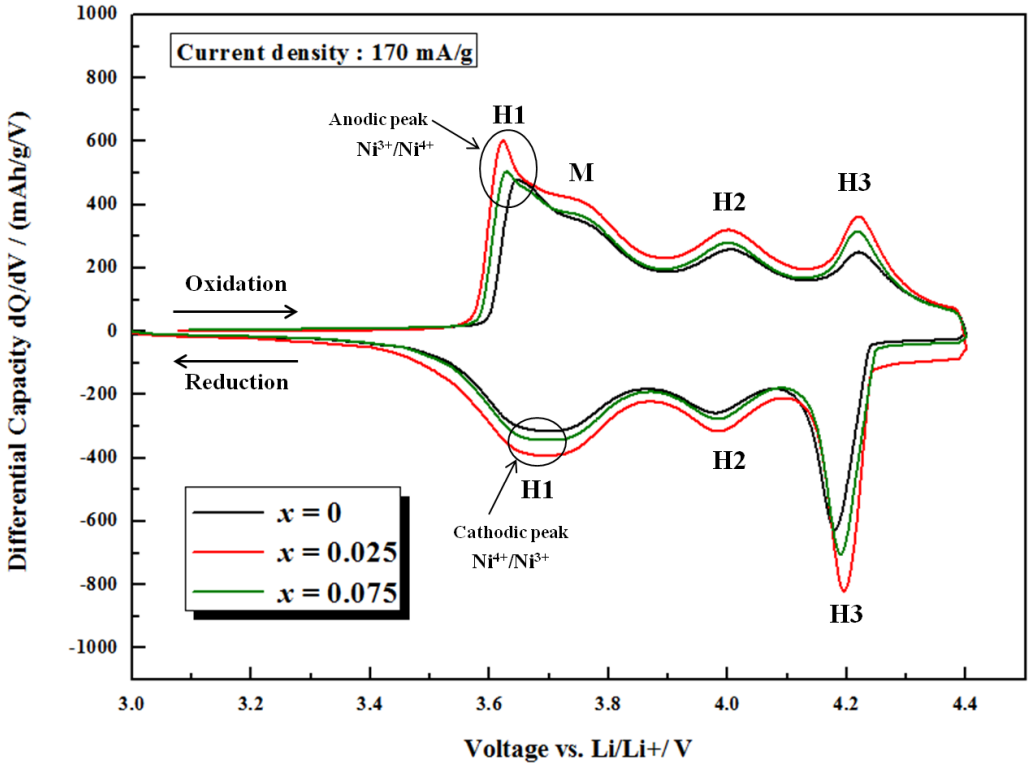

Figure 6. Differential capacity vs voltage of the $LiNi_{0.90-x}Co_{0.05}Al_{0.05}Y_xO_2$ (x = 0, 0.025, 0.075) cells in the voltage range of 3.0~4.4 V at 1.0 C (170 mAg).

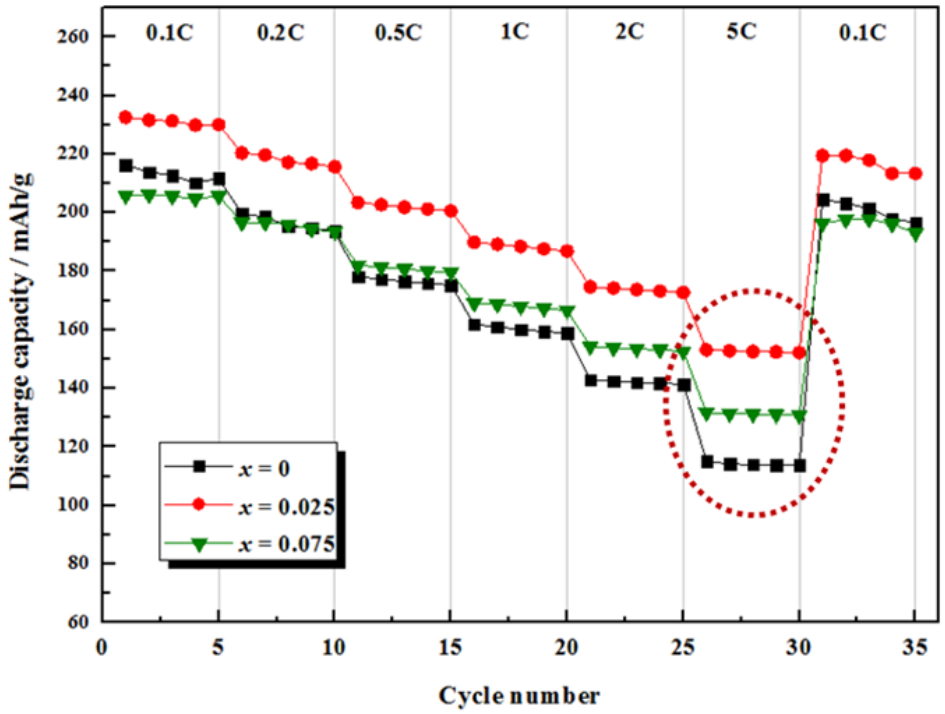

Figure 7. Rate capability curves of the $LiNi_{0.90-x}Co_{0.05}Al_{0.05}Y_xO_2$ (x = 0, 0.025, 0.075) cathodes in the voltage range of 3.0~4.4 V at 0.1C, 0.2C, 0.5C, 1.0, 2.0, 5.0 and 0.1C.

the particle size ranged from 5 to 9 μm. Finally, the particles obtained after 52 hrs of precipitation had a spherical shape.

3.1.3. SEM image studies

Fig. 4 shows SEM images of the (a) $Ni_{0.95}Co_{0.05}(OH)_2$ precursor and $LiNi_{0.90-x}Co_{0.05}Al_{0.05}Y_xO_2$ powders (x = 0, 0.025, 0.075) image series (b)-(d). The $Ni_{0.95}Co_{0.05}(OH)_2$ precursor was prepared by the co-precipitation method. It is obvious that $Ni_{0.95}Co_{0.05}(OH)_2$ powders adopted a spherical morphology in secondary particles and the estimated particle diameter was about 5–9 μm in, while the primary particles adopted a needle-like shaped and were densely agglomerated in secondary forms. As the result of sintering the samples Fig. 4 (b, c, d), the morphology and size of the $LiNi_{0.90}Co_{0.05}Al_{0.05}O_2$ secondary particles calcined at 750 □ for 18 hrs remained almost the same as the precursor. However, the presence of the needle-shaped primary particles of the precursor as to be seen the SEM images clearly indicates that there was a structural change when compared the cylindrically-shaped primary particles of $LiNi_{0.90}Co_{0.05}Al_{0.05}O_2$ powders. The SEM images of pristine (Fig.4(b)) and Y-doped powders (shown in Fig.4(c) and (d)). There was little change in the morphology by Y-doping. The powders had agglomerated, and were consisting of small particles with an average particle size of about 500 nm.

3.2. Electrochemical behavior

3.2.1. Initial charge-discharge studies

Fig. 5 shows the initial charge/discharge curves for the $LiNi_{0.90-x}Co_{0.05}Al_{0.05}Y_xO_2$ (x = 0, 0.025, 0.075) cells in the cut-off voltage 4.4 ~ 3.0 V at 1.0 C. The initial discharge capacity value of the pristine sample was 185.6 $mAhg^{-1}$, and the Y-doped materials delivered an initial discharge capacity of 195.8 and 187.7 $mAhg^{-1}$ for x = 0.025, 0.075, respectively. The capacity retention of the Y-doped samples (~87%) was also better than that of the pristine (~ 82%). The yttrium doping expanded the pathway for Li^+ to intercalate and deintercalate. So, the yttrium doping was correlated with improved discharge capacities of the cathode and better capacity retention during the cycling. Fig. 6 presents differential capacity plots (DCPs) of pristine sample and the Y-doped $LiNi_{0.90}Co_{0.05}Al_{0.05}O_2$ cells at in the cut-off voltage 4.4 ~ 3.0 V at 0.2 C. The DCPs of $LiNi_{0.90}Co_{0.05}Al_{0.05}O_2$ display features characteristic of voltage plateaus during charge process at ~3.65, 3.73, 3.99, and 4.21 V, associated with complete oxidation. The main cathodic peaks at ~3.68, 3.98, and 4.18 V during the discharge process were meanwhile ascribed to the reduction reaction. The major anodic/cathodic peaks at ~3.65/3.68 V correspond to the oxidation/reduction process of Ni^{3+}/Ni^{4+}. The anodic peak at 3.65 V has a shoulder at ~3.73 V, which is a two-phase region corresponding to the phase transition of the hexagonal (H1) to monoclinic (M). Also the anodic/cathodic peaks at 3.99/3.98 V and 4.21/4.18 V were assigned to the phase transition of the monoclinic to hexagonal (H2) and hexagonal (H2) to hexagonal (H3), respectively [22, 23]. On the other hand, the DCPs of Y-doped samples were displayed the voltage plateaus that were almost constant excluding the main anodic peaks at ~3.55 V, due to markedly reduced resistance by Y-doping.

3.2.2. Rate capability studies (C-rate)

Rate capability is one of the most important electrochemical

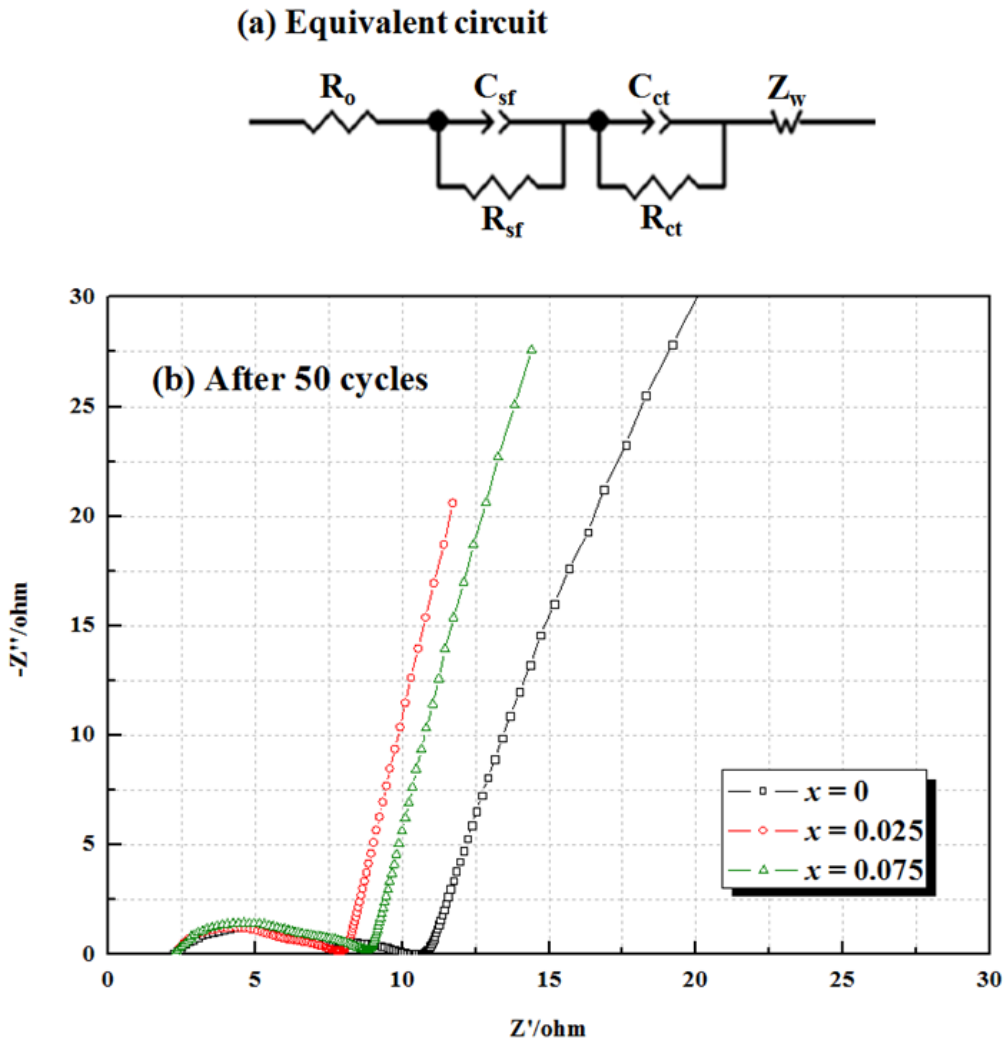

Figure 8. (a) Equivalent circuit and (b) impedance after 50 cycles in the pristine and Y-doped electrodes in coin type half-cells.

characteristics of lithium secondary batteries required for power storage application. Fig. 7 shows the discharge specific capacities of the $LiNi_{0.90-x}Co_{0.05}Al_{0.05}Y_xO_2$ (x = 0, 0.025, 0.075) cathodes. The cells were charged and discharged between maximally 3.0 and 4.4V with charges of 0.1, 0.2, 0.5, 1.0, 2.0, 5.0 and 0.1C, respectively. As shown in Fig. 7, the capacity retention difference between the pristine and Y-doped $LiNi_{0.90}Co_{0.05}Al_{0.05}O_2$ cathode became larger with an increase in the C-rate. For instance, the capacity retentions of $LiNi_{0.90-x}Co_{0.05}Al_{0.05}Y_xO_2$ (x = 0.075) was 95, 81.7 and 63.8% at 0.2, 1.0 and 5.0 C-rate, respectively. Meanwhile the pristine was capacity retentions of 92.2, 75.2 and 53.6% at 0.2, 1.0 and 5.0 C-rate, respectively (see Table 2). It is noticeable that a much lower over potential was observed in the Y-doped samples than in the pristine, especially for x = 0.025 at high C-rates, indicating that the yttrium doping significantly reduced the polarization of the cathode/electrolyte interface in the cell.

Table 2. Capacity retention at various C-rates of the $LiNi_{0.90-x}Co_{0.05}Al_{0.05}Y_xO_2$ powders (x= 0, 0.025, 0.075) (Units are %).

	0.1C	0.2C	0.5C	1C	2C	5C	0.1C
x = 0	100	92.2	82.9	75.2	66.7	53.6	94.3
x = 0.025	100	94.3	87.4	81.5	75.2	66	93.8
x = 0.075	100	95	87.9	81.7	74.7	63.8	95.4

Table 3. Surface-Film Resistance (R_{sf}) and Charge-Transfer Resistance (R_{ct}) for Pristine and Y-doped $LiNi_{0.90}Co_{0.05}Al_{0.05}O_2$ cathodes.

Composition	R_{SEI} (Ω)	R_{ct} (Ω)
x = 0	6.59	4.2
x = 0.025	5.87	1.99
x = 0.075	6.24	2.53

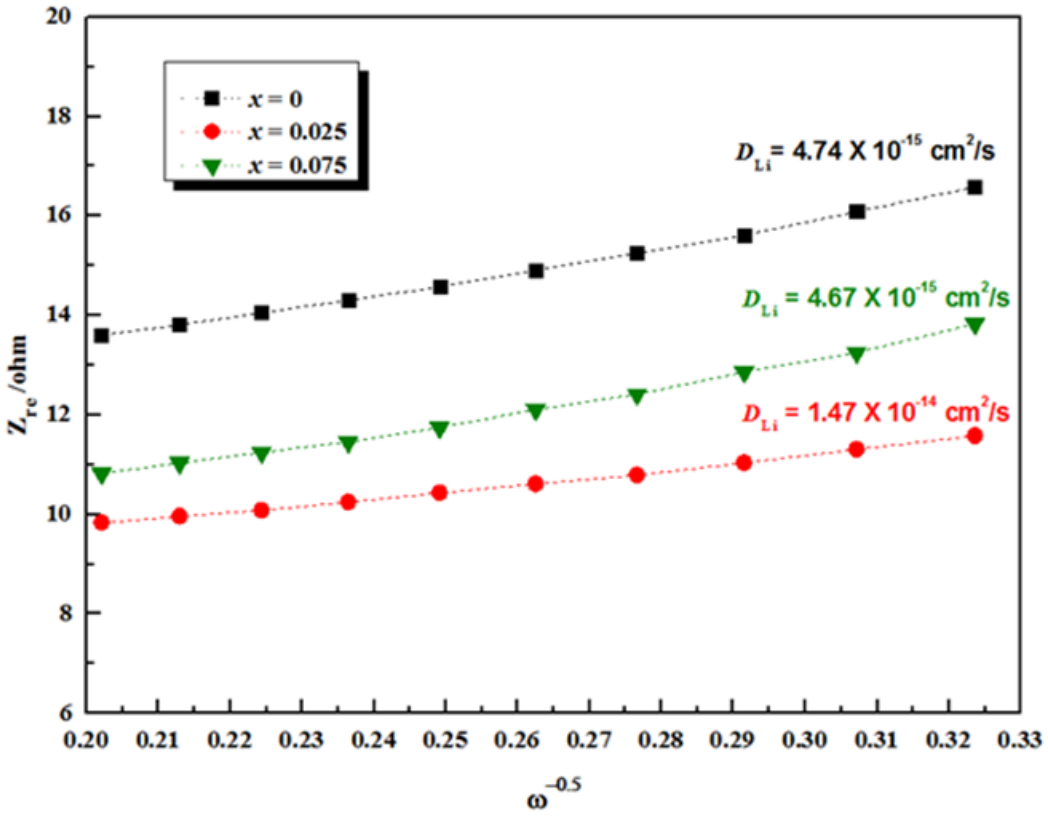

Figure 9. Graph of Z_{re} plotted against $\omega^{-0.5}$ at low frequency region for $LiNi_{0.90-x}Co_{0.05}Al_{0.05}Y_xO_2$ (x = 0, 0.025, 0.075) cathodes.

3.2.3. Electrochemical impedance spectroscopy (EIS)

Fig. 8 shows the impedance spectra of the $LiNi_{0.90-x}Co_{0.05}Al_{0.05}Y_xO_2$ (x = 0, 0.025, 0.075) samples before and after 50 cycles with a charge of 1.0C (170 mA/g). An equivalent circuit was used interpret the impedance results (Fig. 8a). R_o and R_{Sf} are the ohmic resistance of the cell and the surface film-covered electrode particles, respectively. R_{ct} is the charge-transfer resistance at the electrode and electrolyte [24-26]. Generally, impedance spectra for lithium battery test cells containing cathode material exhibit two semicircles and a line inclined at a constant angle to the real axis. The semicircle occurring at a high frequency could be attributed to the resistance of the surface film (R_{sf}). The R_{sf} of $LiNi_{0.90-x}Co_{0.05}Al_{0.05}Y_xO_2$ (x = 0, 0.025, 0.075) was measured to 6.59, 5.87, and 6.24 Ω, respectively and the R_{ct} of Y-doped samples had also a lower value than that of bare sample after 50 cycles, the R_{ct} value of the pristine sample was 4.2 Ω after 50 cycles. On the contrary, the R_{ct} of the Y-doped $LiNi_{0.90-x}Co_{0.05}Al_{0.05}Y_xO_2$ (x = 0.025, 0.075) electrodes were 1.99, and 2.53 Ω after 50 cycles (Table 3). The resistance of the Y-doped samples is the lowest after 50 cycles, which mean that the increase of crystal parameter will allow Li^+ to more easily intercalate/deintercalate. Therefore, the improved rate capability of Y-doped samples may be due to an extension of the pathway for Li^+ ion and reduction in charge transfer resistance.

The EIS can be used to calculate the lithium diffusion coefficient (D_{Li}) using the following equation [27, 28].

$$Z_{re} = R_{ct} + R_s + \sigma\omega^{-0.5} \quad (1)$$

$$D_{Li} = 0.5\left(\frac{RT}{AF^2\sigma_W C}\right)^2 \quad (2)$$

where the meanings of R_{ct} is charge transfer resistance, Re the electrolyte resistance, ω the angular frequency in the low frequency region, D the diffusion coefficient, R the gas constant, T the absolute temperature, F the Faraday's constant, A the area of the electrode surface, and C the molar concentration of Li^+ ions (moles cm^{-3}) [29]. The plot of the Z_{re} vs. the reciprocal square root of the lower angular frequencies is illustrated in Fig. 9. The lithium diffusion coefficients of Y-doped $LiNi_{0.90-x}Co_{0.05}Al_{0.05}Y_xO_2$ (x = 0, 0.025, 0.075) were calculated to be 4.74×10^{-15}, 1.47×10^{-14} and 4.67×10^{-15} cm^2 s^{-1}, respectively. It can be found that $LiNi_{0.875}Co_{0.05}Al_{0.05}Y_{0.025}O_2$ has the highest lithium diffusion coefficient among three samples. The lowest lithium diffusion coefficient of $LiNi_{0.825}Co_{0.05}Al_{0.05}Y_{0.075}O_2$ may be due to the much impurity (see Fig. 1), and then hinder the migration of lithium ions, but this was exhibit much better electrochemical performance than the pristine sample at high C-rates (see Fig. 7). This is related to better cation mixing by Y-doping than the pure $LiNi_{0.90}Co_{0.05}Al_{0.05}O_2$.

4. CONCLUSIONS

In this study, we have successfully prepared layered $LiNi_{0.90}Co_{0.05}Al_{0.05}O_2$ cathodes by co-precipitation, then yttrium oxide have synthesized by solid-state method and the synthesized material was characterized. All peaks can be identified as a hexagonal lattice of α-$NaFeO_2$ type. However, some low intensity bands appear while the amount of doping Y^{3+} ions increase to a high level, which was attributed to the forming of Y_2O_3 phase. After doping, the lattice parameter 'c' becomes large. It is demonstrated that the Y^{3+} substitution for Ni^{2+} in $LiNi_{0.90-x}Co_{0.05}Al_{0.05}Y_xO_2$ electrodes improved the Li^+-diffusion. Moreover, the $LiNi_{0.875}Co_{0.05}Al_{0.05}Y_{0.025}O_2$ has the best rate capability among all the samples, especially when they were tested under the high current density (at 5.0 C). From EIS measurements, it is clearly found that Y-doping improves reversibility of the electrode reactions and restraining the increase of charge transfer resistance of cathode during cycling, which results in the improved rate capability.

5. ACKNOWLEDGMENTS

This research was supported by the Global Excellent Technology Innovation of the Korea Institute of Energy Technology Evaluation and Planning (KETEP), granted financial resource from the Ministry of Trade, Industry & Energy, Republic of Korea(No. 20135020900010), and Regional Innovation Center (RIC) Program funded by the Ministry of Trade, Industry and Energy (MOTIE) and Korea Institute for Advancement of Technology (KIAT) through the Promoting Regional specialized Industry.

REFERENCES

[1] C.S. Kang, J.T. Son, J. Electroceram., 29, 235 (2012).
[2] J.T. Son, H.G. Kim, J. Power Sources, 147, 220 (2005).
[3] M.K. Kim, H.T. Chung, Y.J. Park, J.G. Kim, J.T. Son, K.S. Park, H.G. Kim, J. Power Sources, 99, 34 (2001).
[4] J.T. Son, E.J. Cairns, Electrochem. Solid-State Letters, 9, A27 (2006).
[5] C.S. Kang, C. Kim, T.J. Park, J.T. Son, Chem. Letters, 41, 1428 (2012).
[6] J.T. Son, H.G. Kim, Y.J. Park, Electrochim. Acta, 50, 453 (2004).
[7] S.M. Lee, S.H. Oh, J.P. Ahn, W.I. Cho, H. Jang, J. Power Sources, 159, 1334 (2006).
[8] X.X. Shia, C.W. Wang, X.L. Ma, J.T. Suna, Mater. Chem. Phys., 113, 780 (2009).
[9] Jiangfeng Xiang, Caixian Chang, Feng Zhang, Jutang Sun, J. Alloy. Compd., 475, 483 (2009).
[10] G.H. Kim, S.T. Myung, H.S. Kim, Y.K. Sun, Electrochim. Acta, 51, 2447 (2006).
[11] H. Li, G. Chen, B. Zhang, J. Xiu, Solid Sate Commun., 146, 115 (2008).
[12] P.Y. Liao, J.G. Duh, H.S. Sheu, J. Power Sources, 183, 766 (2008).
[13] C.Q. Xu, Y.W. Tian, Y.C. Zhai, L.Y. Liu, Mater. Chem. Phys., 98, 532 (2006).
[14] G.V. Subba Rao, B.V.R. Chowdari, H.J. Lindner, J. Power Sources. 313, 97–98 (2001).
[15] R.V. Mangalaraja, J. Mouzon, P. Hedstrom, I. Kero, K.V.S. Ramam, C.P. Camurri, M. Oden, J. Mater. Process. Technol., 208, 415 (2008).
[16] S.T. Myung, K. Izumi, S. Komaba, Y.K. Sun, H. Yashiro, N. Kumagai, Chem. Mater., 17, 3695 (2005).
[17] S.T. Myung, K. Izumi, S. Komaba, H. Yashiro, H.J. Bang, Y.K. Sun, N. Kumagai, J. Phys. Chem., 111, 4061 (2007).
[18] J.A. Dean, Lange's Handbook of Chemistry, fifteenth ed., McGraw-Hill, Inc., USA, 1999.
[19] T. Ohzuku, A. Ueda, M. Nagayama, J. Electrochem. Soc., 140, 1862 (1993).
[20] G.T.K. Fey, J.G. Chen, V. Subramanian, T. Osaka, J. Power Sources, 112, 384 (2002).
[21] J.R. Reimers, E. Rossen, C.D. Jones, J.R. Dahn, Solid State Ionics, 61, 335 (1993).
[22] Daocong Li, Zhenghe Peng, Wenyong Guo, Yunhong Zhou, J. Alloy. Compd., 457, L1 (2008).
[23] L. Kavan, M. Gratzel, Electrochem. Solid State Lett., 5, A39 (2002).
[24] Y.H. Cho, J.P. Cho, J. The Electrochem. Society, 157, 625 (2010).
[25] C.S. Kang, J.T. Son, J. KIEEME. 24, 850 (2011).
[26] C. Kim, C.S. Kang, J.T. Son, J. Korea. Electrochem. Soc., 15, 95 (2012).
[27] G.Q. Liu, H.T. Kuo, R.S. Liu, C.H. Shen, D.S. Shy, X.K. Xing, J.M. Chen, J. Alloys Compd., 496, 512 (2010).
[28] Q. Cao, H.P. Zhang, G.J. Wang, Q. Xia, Y.P. Wu, H.Q. Wu, Electrochem. Commun., 9, 1228 (2007).
[29] A.J. Bard, L.R. Faulkner, Electrochemical Methods, second ed., John Wiley&Sons, New York, 2001.
[30] T. Ohzuku, A. Ueda, M. Kouguchi, J. Electrochem. Soc., 142, 4033 (1995).
[31] C. Delmas, I. Saadoune, Solid State Ionics. 53–56,370 (1992).
[32] C. Delmas, I. Saadoune, A. Rougier, J. Power Sources, 43, 595 (1993).
[33] E. Zhecheva, R. Stoyanova, Solid State Ionics, 66, 143 (1993).